

7-1-2012

Plasmodium falciparum SSB Tetramer Wraps Single-Stranded DNA with Similar Topology but Opposite Polarity to *E. coli* SSB

Edwin Antony

Marquette University, edwin.antony@marquette.edu

Elizabeth A. Weiland

Washington University School of Medicine in St. Louis

Sergey Korolev

Saint Louis University - Main Campus

Timothy M. Lohman

Washington University School of Medicine in St. Louis

Accepted version. *Journal of Molecular Biology*, Vol. 420, No. 4-5 (July 2012): 269-283. [DOI](#).

Edwin Antony was affiliated with Washington University at time of publication.

NOTICE: this is the author's version of a work that was accepted for publication in *Journal of Molecular Biology*. Changes resulting from the publishing process, such as peer review, editing, corrections, structural formatting, and other quality control mechanisms may not be reflected in this document. Changes may have been made to this work since it was submitted for publication. A definitive version was subsequently published in *Journal of Molecular Biology*, VOL 420, ISSUE 4-5, July 2012, [DOI](#).

Plasmodium falciparum SSB Tetramer Wraps Single Stranded DNA with Similar Topology but Opposite Polarity to *E. coli* SSB

Edwin Antony

*Department of Biochemistry and Molecular Biophysics,
Washington University School of Medicine
St. Louis, MO*

Elizabeth A. Weiland

*Department of Biochemistry and Molecular Biophysics,
Washington University School of Medicine
St. Louis, MO*

Sergey Korolev

*Edward A. Doisy Department of Biochemistry and Molecular
Biology, Saint Louis University School of Medicine
St. Louis, MO*

Timothy M. Lohman

*Department of Biochemistry and Molecular Biophysics,
Washington University School of Medicine
St. Louis, MO*

Abstract: Single stranded DNA binding (SSB) proteins play central roles in genome maintenance in all organisms. *Plasmodium falciparum*, the causative agent of malaria, encodes an SSB protein that localizes to the apicoplast and likely functions in the replication and maintenance of its genome. *Pf*-SSB shares a high degree of sequence homology with bacterial SSB proteins, but differs in the composition of its C-terminus, which in *E. coli* SSB interacts with more than a dozen other proteins. Using sedimentation methods we show that *Pf*-SSB forms a stable homo-tetramer alone and when bound to single stranded DNA. We also present a crystal structure at 2.1 Å resolution of the *Pf*-SSB tetramer bound to two (dT)₃₅ molecules. The *Pf*-SSB tetramer is structurally similar to the *E. coli* SSB tetramer and ssDNA wraps completely around the tetramer with a "baseball seam" topology that is similar to *E. coli* SSB in its "65 binding mode". However, the polarity of the ssDNA wrapping around *Pf*-SSB is opposite to that observed for *E. coli* SSB. The interactions between the bases in the DNA and the amino acids side chains also differ from those observed in the *E. coli* SSB-DNA structure suggesting that other differences may exist in the DNA binding properties of these structurally similar proteins.

Keywords: DNA repair, recombination, replication, structure, *Plasmodium*, malaria

Introduction

Plasmodium falciparum is a eukaryotic parasite and the causative agent for over 250 million cases of malaria that result in five million deaths annually¹. It contains a unique non-photosynthetic plastid-like organelle called the apicoplast, which is involved in a variety of biosynthetic pathways of the parasite. A single apicoplast is present in each cell and functions in isoprenoid, fatty acid and heme synthesis/metabolism and is critical to parasite survival and pathogenesis making it a logical target for anti-malarial drugs. The ~35 kb apicoplast genome contains 68 open reading frames which encode a variety of ribosomal proteins, tRNAs, RNA polymerase, chaperones and other proteins of unknown function². However, proteins involved in DNA metabolism are encoded by the nuclear DNA and targeted for transport to the apicoplast by an apicoplast localization signal (ALS) which is cleaved upon delivery to the apicoplast³. The single stranded (ss) DNA binding (SSB) protein from *P. falciparum* (*Pf*-SSB) is encoded in the nucleus and transported to the apicoplast where it likely functions in the replication and maintenance of the apicoplast genome⁴.

SSB proteins are present in nearly all organisms and bind to ssDNA intermediates produced transiently during replication, repair and recombination. *E. coli* SSB (*Ec*-SSB) is a well characterized prototype of bacterial SSB proteins⁵ and shares high sequence homology with *Pf*-SSB (39 % identity and 66 % homology)⁴. *Ec*-SSB functions as a homo-tetramer with each subunit consisting of two domains, an N-terminal OB-fold containing the ssDNA binding site and an unstructured C-terminal tail. *Ec*-SSB also interacts with more than a dozen other proteins involved in DNA metabolism⁸. These interactions are primarily mediated through a conserved stretch of 8–10 amino acids located at the end of its unstructured C-termini⁸.

In the case of *Ec*-SSB, it has been shown that at moderate to high salt concentrations a ssDNA ~65 nucleotides long can fully wrap around the tetrameric DNA binding core to form the so-called (SSB)₆₅ binding mode¹¹. However, due to its four potential DNA binding sites, *Ec*-SSB can also bind to long ssDNA in a number of different binding modes that differ by the number of subunits (OB-folds) within the tetramer that contact the DNA. In the (SSB)₆₅ mode ssDNA interacts with all four subunits and displays little tendency to form cooperative clusters along ssDNA. The low cooperative, fully wrapped (SSB)₆₅ binding mode has been proposed to facilitate RecA mediated DNA strand exchange during homologous recombination. In fact, *Ec*-SSB, while bound in its (SSB)₆₅ mode is able to diffuse along ssDNA and transiently melt DNA hairpins, thus facilitating RecA filament formation along ssDNA¹⁸. Here we present a structural study of the *Pf*-SSB protein and its complexes with ssDNA including a crystal structure of a *Pf*-SSB tetramer in complex with ssDNA in a fully wrapped binding mode allowing a detailed comparison of its structure with *Ec*-SSB.

Results

Pf-SSB forms a stable homo-tetramer in solution

SSB proteins can exist in a variety of oligomeric states including monomers (e.g., T4 phage gp32)¹⁹, dimers (e.g., *D. radiodurans* SSB)²⁰, trimers (e.g., eukaryotic RPA)²¹, tetramers (most bacterial SSBs)⁸ and pentamers (e.g., *D. radiodurans* DdrB)²². Based on dynamic light scattering and sucrose density gradient analysis, a

histidine tagged version of recombinant *Pf*-SSB appears to behave as a homo-tetramer in solution⁴. Here, we examined the assembly state of an untagged version of *Pf*-SSB using analytical sedimentation methods. In sedimentation velocity experiments of *Pf*-SSB in the absence of reducing agents (3 μ M *Pf*-SSB, buffer H^{0.2} at 25°C), we observe three or more distinct species with average sedimentation coefficients of 5.3 ± 0.2 , 8.1 ± 0.4 and 11.2 ± 0.7 S with predicted molecular weights corresponding to a tetramer (92.7 kDa), octamer (176 kDa) and dodecamer (280 kDa; [Figure S1A](#)). Since *Pf*-SSB has a native cysteine at position 93, we tested whether disulfide bond formation influences the oligomerization by repeating the experiments in the presence of reducing agents (either 5 mM 2-mercaptoethanol (2-ME) or 1 mM tris(2-carboxyethyl)phosphine(TCEP)). In the presence of reducing agents in buffer H^{0.2}, *Pf*-SSB displays a single symmetrical peak in a continuous sedimentation [c(s)] analysis consistent with a single species ([Figure S1b](#)), with a weight average sedimentation coefficient of 5.28 ± 0.16 S, corresponding to a predicted molecular weight of 92.5 kDa and a frictional coefficient ratio, $f/f_0 = 1.39 \pm 0.03$. This is close to the expected molecular weight for a *Pf*-SSB homo-tetramer (98,296 Da) as calculated from its amino acid composition.

We also used sedimentation equilibrium to obtain a rigorous molecular weight estimate of *Pf*-SSB. The results of experiments performed at three *Pf*-SSB concentrations (1.04, 3.13 and 6.03 μ M (tetramer)) and four speeds (9.5, 11.5, 14 and 17 k rpm) are shown in [Figure 1B](#). Global non-linear least squares (NLLS) analysis of these data gave results consistent with a single ideal species ([eq 1](#), Methods section) with an average molecular mass of $M_r = 98824 \pm 221$ Da. This value agrees well with the predicted molecular weight of 98296 Da for a *Pf*-SSB homo-tetramer. Hence *Pf*-SSB is a stable homo-tetramer over a concentration range from 0.5–6 μ M (tetramer).

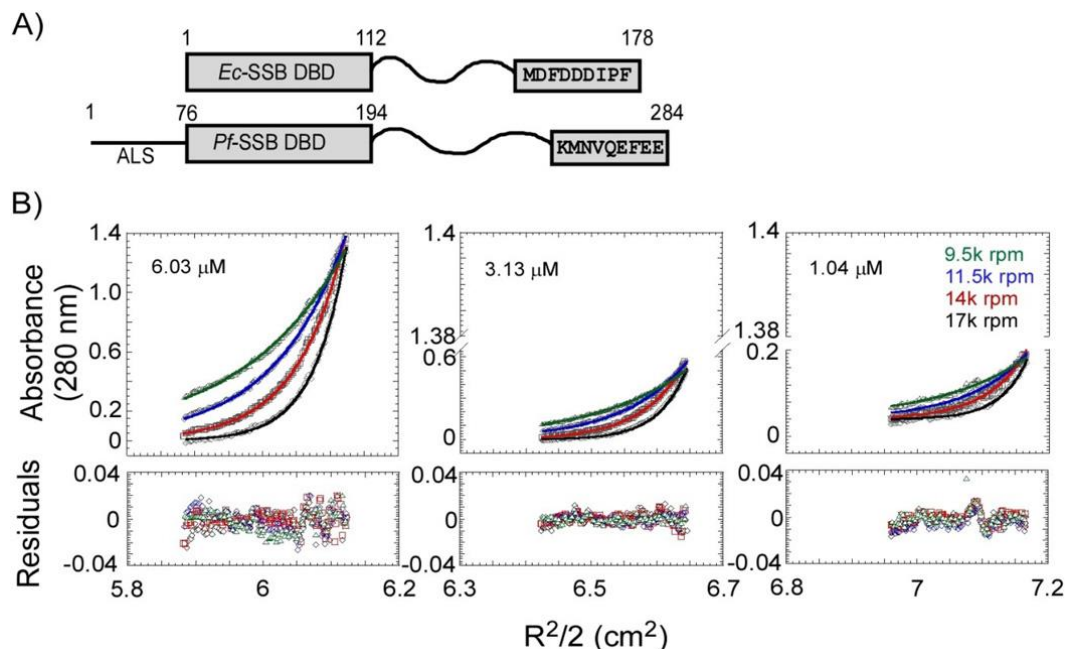


Figure 1: Pf-SSB is a stable homotetramer in solution

(A) Domain architecture of Pf- and Ec-SSB proteins. (B) Sedimentation equilibrium experiments indicate that Pf-SSB is a stable homotetramer in solution. Experiments were performed at three different protein concentrations as indicated in the plot, and at four rotor speeds (9.5 k – green, 11.5 k – blue, 14 k – red and 17 k – black). The smooth black lines depict the fits to a single-species model and the appropriate residuals are also shown.

Pf-SSB binds tightly to ssDNA

Ec-SSB contains 4 Trp residues per monomer (3 in the DNA binding core) and ssDNA binding can be monitored by the quenching of its intrinsic Trp fluorescence (~90% at saturation). The *Ec-SSB* tetramer binds to DNA with very high affinity and 65 nucleotides of poly (dT) are required to fully wrap around the tetramer¹⁰. As such, an *Ec-SSB* tetramer can bind either one molecule of (dT)₇₀ or two molecules of (dT)₃₅²⁶. *Pf-SSB* contains 3 Trp residues per monomer in the same conserved positions within the DNA binding core and its Trp fluorescence is also quenched upon binding ssDNA (see below). For *Pf-SSB*, we have measured an occluded site size of 62 ± 2 nucleotides per *Pf-SSB* tetramer on poly (dT) at high [NaCl] (> 0.2 M) (Antony *et al.*, accompanying paper). In preparation for attempts at crystallizing *Pf-SSB* with ssDNA, we examined the binding of *Pf-SSB* to both (dT)₇₀ and (dT)₃₅ by monitoring the accompanying change in *Pf-SSB* tryptophan fluorescence (buffer H^{0.2} at 25°C) as shown in [Figure 2A and B](#). These titrations show that under these conditions, *Pf-SSB* binds

very tightly to both (dT)₇₀ and (dT)₃₅ such that we can only estimate a binding stoichiometry, but not an affinity. The *Pf*-SSB tetramer can bind either one molecule of (dT)₇₀ (Figure 2A) or two molecules of (dT)₃₅ (Figure 2B) per tetramer and in both cases almost complete quenching (96 – 98 %) of the Trp fluorescence is observed. By comparison with the Trp fluorescence quenching observed for (dT)₇₀ and (dT)₃₅ binding of *Ec*-SSB, these results suggest that one molecule of (dT)₇₀ or two molecules of (dT)₃₅ can bind to *Pf*-SSB, both resulting in complete wrapping of DNA around the *Pf*-SSB tetramer. One interesting difference between *Pf*-SSB and *Ec*-SSB is the lack of apparent negative cooperativity in the binding of the second molecule of (dT)₃₅ to the *Pf*-SSB tetramer (see Antony *et al.*, accompanying paper), whereas *Ec*-SSB tetramer shows clear negative cooperativity.

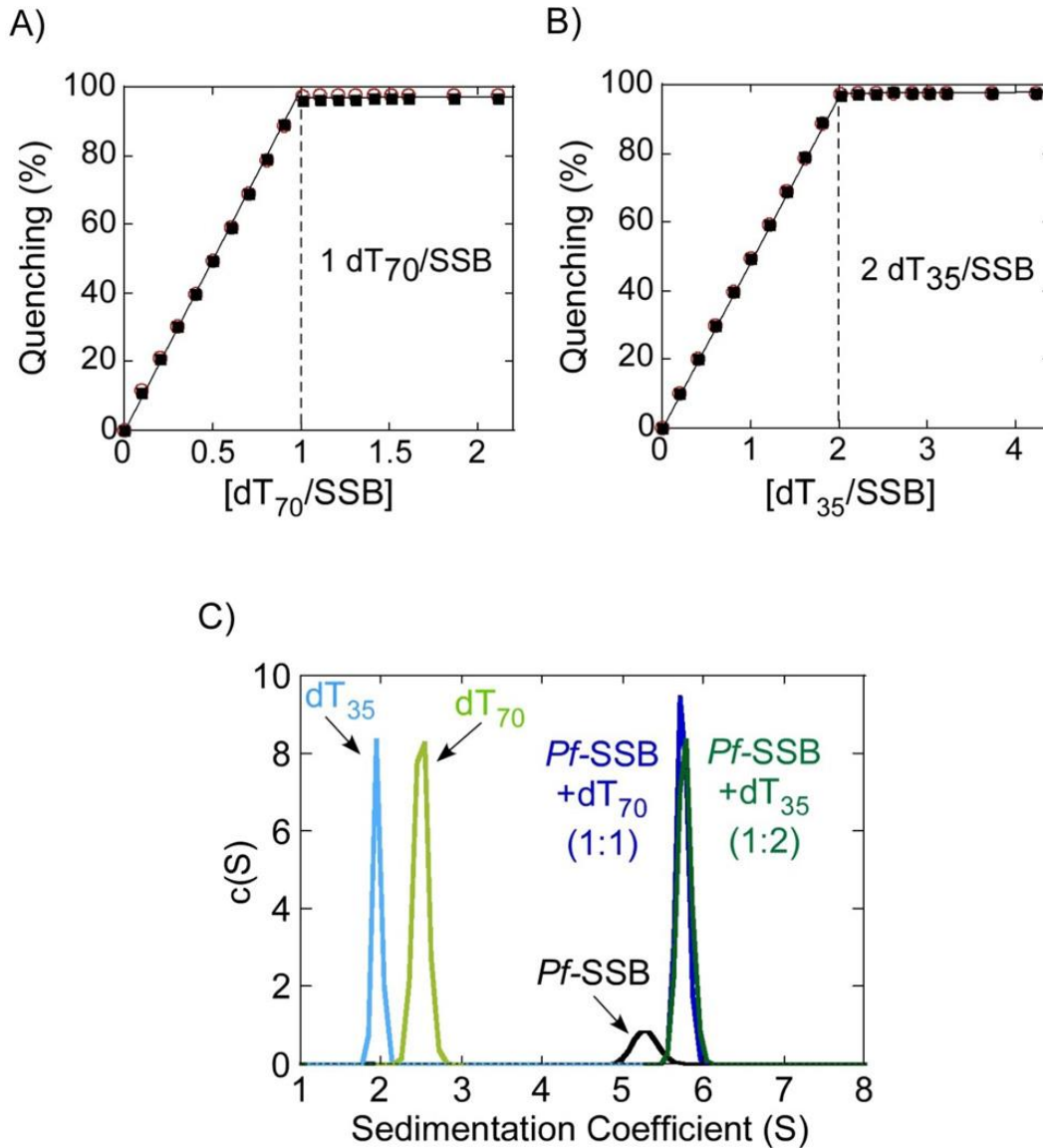


Figure 2: Pf-SSB binds stoichiometrically to DNA

Fluorescence experiments show the quenching of tryptophan fluorescence upon binding to (dT)₇₀ (A) or (dT)₃₅ (B) DNA oligonucleotides. The dotted lines show the stoichiometric binding of either one (dT)₇₀ or two (dT)₃₅ molecules per *Pf*-SSB tetramer. (○) and (■) represent experiments done at either 0.1 μM or 0.3 μM *Pf*-SSB in the reaction respectively. (C) Continuous sedimentation coefficient distribution *c*(s) analysis of *Pf*-SSB in the presence or absence of ssDNA. *Pf*-SSB sediments as a single tetramer in the absence of DNA (green) and is capable of stoichiometrically binding two (dT)₃₅ molecules (when mixed in a 1:2 ratio, dark green trace) or one (dT)₇₀ molecule (mixed in a 1:1 ratio, dark blue). Sedimentation profiles of (dT)₃₅ (light green) or (dT)₇₀ (light blue) in the absence of protein are also depicted.

We also examined *Pf*-SSB and its ssDNA complexes using sedimentation velocity. *Pf*-SSB tetramers, when bound to either two molecules of (dT)₃₅ or one molecule of (dT)₇₀, displayed *c*(s) profiles²³

with single symmetrical peaks with $\bar{s}_{20,w} = 5.73 \pm 0.07$ S and 5.76 ± 0.09 S, respectively (Figure 2C), corresponding to predicted molecular weights of 133.6 and 133.58 kD, respectively. The f/f_0 values calculated from these experiments are 1.39 ± 0.02 , 1.63 ± 0.02 and 1.63 ± 0.03 for *Pf*-SSB alone and the *Pf*-SSB-(dT)₃₅ and *Pf*-SSB-(dT)₇₀ complexes, respectively. Therefore, *Pf*-SSB bound to either one (dT)₇₀ or two (dT)₃₅ molecules displays similar hydrodynamic properties.

Crystal Structure of Pf-SSB is similar to E. coli SSB

We have solved a crystal structure at 2.1 Å resolution of *Pf*-SSB in complex with two molecules of (dT)₃₅. The *Pf*-SSB used in the crystallization contained amino acid residues 77–284. Residues 1–76 are part of the apicoplast localization signal (Figure 1A) and are cleaved upon arrival at the apicoplast, hence we did not include these in the recombinant protein that we expressed and purified. We observed two crystal forms with either a monomer or a tetramer in the asymmetric unit (Figure S2). In both cases, we only observe electron density for the amino acids that form the DNA binding core (residues 77–194). Upon analysis of the crystals using SDS-PAGE, the protein component that had crystallized migrated faster than the full length starting protein suggesting that the C-terminal part of the protein was at least partially cleaved (Figure S2 C). Since we observe excellent density for residues 77–194, the cleavage must occur after residue 194; however, we have not determined the precise site of cleavage. Similar proteolytic cleavage has been observed during crystallization of the *Ec*-SSB protein. Since the structural details of both *Pf*-SSB-(dT)₃₅ crystal forms are similar, we discuss only the structure derived from the crystal form showing the tetramer in the asymmetric unit.

Each subunit contains an oligosaccharide/oligonucleotide-fold (OB-fold) found in many SSB proteins³⁴ (Figure 3A), and is composed of five beta strands ($\beta 1$ – $\beta 5$) and one alpha helix (α) connected by short linkers (L1–1', L1'–2, L2–3, L3– α , L α –4, L4–4', L4–5, and L5–5'; Figure 3B). All four subunits in the tetramer have similar conformations with RMSD values ranging from 0.12 to 0.26 Å for 90–95 Ca atoms. The overall structure resembles the *Ec*-SSB tetramer and 77 Ca atoms of *Pf*-SSB and *Ec*-SSB monomers align with RMSD of 0.8 Å (Figure 3C). Alignment was performed using Py Mol with the default

cutoff level of 2 Å. Noticeable differences in the *Pf*-SSB structure are the more ordered 4–5 and 2–3 β-sheets and the disordered tips of the 4–5 loops (Figure 3C). *Pf*-SSB and *Ec*-SSB tetramers align with RMSD of 8.6 Å for 306 Ca atoms reflecting minor differences in the mutual orientation of individual subunits (Figure S3). Both proteins show a high degree of structural similarity in the overall architecture of the DNA binding domains and the organization of the homotetramer.

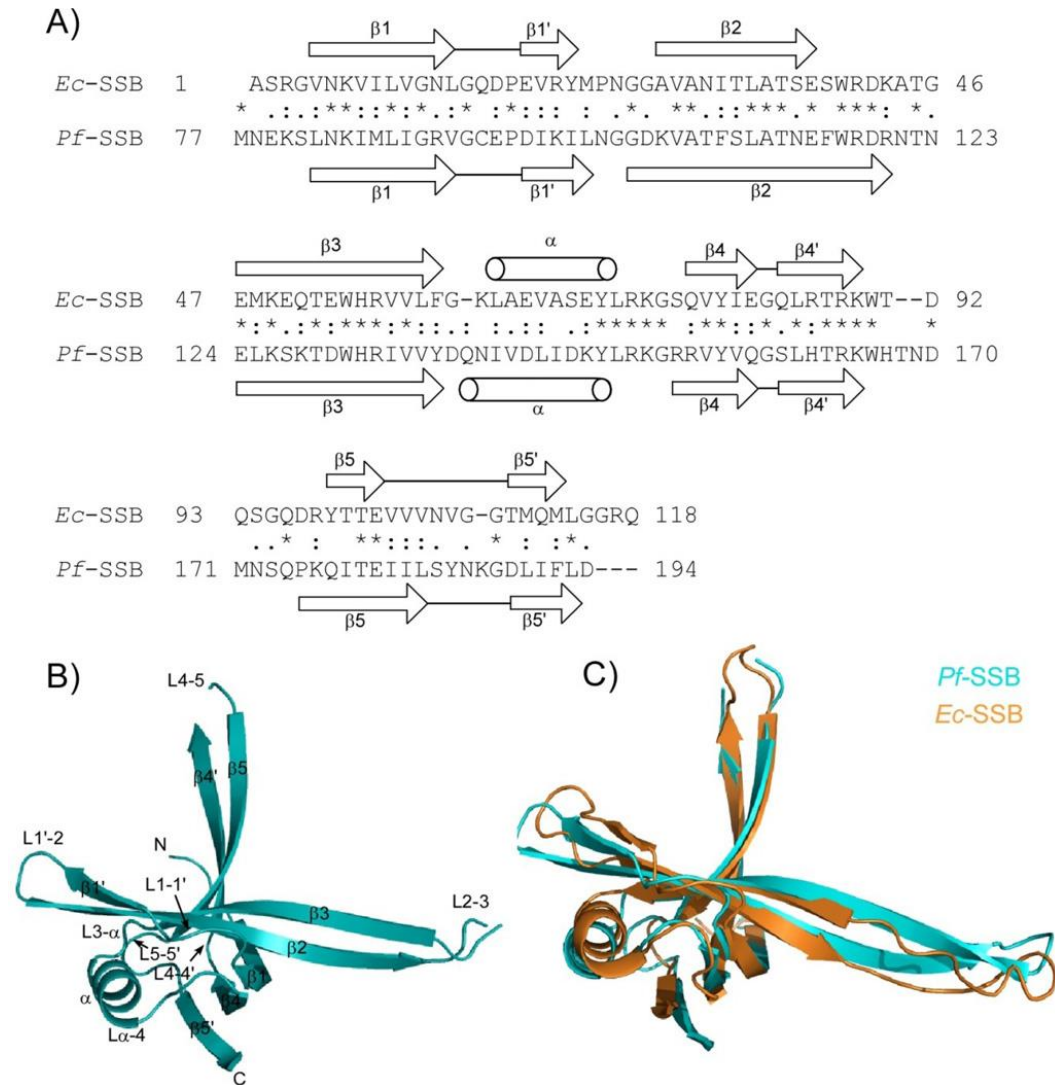


Figure 3 Crystal structure of *Pf*-SSB

(A) Sequence alignment of *Pf*-SSB and *Ec*-SSB and a schematic representation of their secondary structure. Strictly conserved residues are marked by an asterisk (*). (B) Architecture of a single monomer in *Pf*-SSB. (C) Overlay of a single monomer from *Pf*-SSB (cyan) and *Ec*-SSB (orange) highlight the similarity in protein structure between the two proteins.

ssDNA wraps around the Pf-SSB tetramer interacting with all four subunits

Since *Pf*-SSB binds tightly to either one molecule of (dT)₇₀ or two molecules of (dT)₃₅ (Figure 2), we formed and obtained crystals of each of these complexes. Crystals of *Pf*-SSB with two bound (dT)₃₅ molecules diffracted to 2.1Å, although interpretable density is observed for only 25 nts per (dT)₃₅ molecule (Figure 4A), and a majority of the modeled DNA is well ordered (Figure S4). We have numbered the nucleotides T₁ – T₁₄ and T₁₈ – T₂₈ (Figure 4B) (since the DNA is an oligo-(dT), T-1 may not be the actual 5' end of the DNA molecule). We assumed that the gap between the two ordered ssDNA segments was missing three nucleotides based on the distance between the ends of the ssDNA segments and the presence of weak electron density potentially corresponding to the missing nucleotides. Although we observe some density consistent with two or three bases corresponding to residues T₁₅–T₁₇, the density cannot be fit to a single conformation, suggesting that this region is disordered. We also obtained small crystals that diffracted to 3.8 Å for *Pf*-SSB bound to a molecule of (dT)₇₀, but were unable to obtain a structure of this complex due to the poor quality of the crystals. These crystals were of the same space group as the *Pf*-SSB-(dT)₃₅ complex suggesting that (dT)₇₀ is bound in a similar conformation to that of the two (dT)₃₅ molecules.

with respect to nucleotides T1–T3 (C), T4 – T5 (D), T6 and T8 (E), T9 and T13: front view (F), back view (G), (F). The orange spheres denote density for either water or probable ion molecules in the structure that mediate specific interactions between the protein and the DNA.

Protein-DNA contacts

In the *Pf*-SSB-(dT)₃₅ structure, the residues that contact the DNA are identical in all four subunits ([Figure 4](#)). This differs from the asymmetric contacts observed in the *Ec*-SSB-(dC)₃₅ structure¹¹. A schematic of the specific contacts between amino acids in one monomer and the DNA is shown in [Figure 4B](#). Residues from three different subunits contact each half of the (dT)₃₅ molecule. We also observe density for several water and/or ion molecules; since it is difficult to distinguish between electron density for water molecules versus ions at 2.1 Å resolution, all solvent molecules in the structure are modeled and discussed as waters. The first nucleotide in the DNA for which we observe density, denoted T-1, contacts both the 2–3 loop of one subunit and the 1–2 loop of the adjacent subunit. R164 and Y137 contact T-1 through a water molecule and H162 and W117 (subunit I) form stacking interactions with T-1. D130 contacts both T-1 and H162 through water molecules. S184 contacts both the backbone phosphate and the sugar moiety ([Figure 4 C](#)). T-2 makes a contact with K98 through another water molecule and T-3 contacts N101 ([Figure 4 D](#)). R164 also contacts both the T-4 and T-5 base and their respective sugars along with its aforementioned contact with T-1. R133 contacts T-4 and forms a network with E180, R164 and the DNA. Two threonines (T163 and T179) from subunit I coordinate the T-5 and T-6 bases through two waters and the backbone of T-6 makes a contact with S110 ([Figure 4E](#)). W166 forms a stacking interaction with T-5 and this conserved residue assists in bending of the DNA around the individual monomer. W131 is homologous to the functionally critical W54 in *Ec*-SSB³⁸, and makes a base-stacking interaction with T-8. W131 also makes a polar contact with T-6 at which point the DNA bends around the 1–2 loop and funnels towards the other half of the subunit ([Figure 4E](#)).

S110 contacts T-8, N114 and T129 contacts T-9 and along with E79 from subunit I interacts with the bend in the DNA formed by residues T-8 through T-10. T-12 and T-13, the last two residues for which we observe electron density interact with the N-terminus of

subunit I (E79 and K80) and the C-terminus of the subunit IV (R153, D189 and F192). Together with R154 they form a series of well networked connections that may control the entry of the DNA into the next subunit ([Figures 4F and G](#)).

Topology of DNA wrapping around the Pf-SSB tetramer

Although we were unable to solve a structure of the *Pf*-SSB tetramer bound to (dT)₇₀, we were able to use the structure of the complex with two (dT)₃₅ molecules bound to identify the most likely path of the ssDNA in a fully wrapped complex ([Figure 5A](#)). There are four DNA fragments in our structure that show clear electron density for 13–14 nts bound per subunit ([Figure 5B](#)). We observe weak density for 2–4 nts that lie between the DNA fragments bound to subunits I and II and between subunits III and IV ([Figure 5B](#)) and the spacing in these gaps is small (< 18 Å). Hence we assume that these short gaps reflect disordered regions of the two (dT)₃₅ molecules ([Figure 5B](#)). We next need to decide the path that a (dT)₇₀ molecule would follow in a fully wrapped structure. The 3' end of the DNA bound to subunit I and the 5' end of the DNA bound to subunit III would likely be connected if part of a (dT)₇₀ molecule since the ends are unobstructed in the structure and the distance between them is ~ 30 Å ([Figures 5A and 5B](#)). Based on this, a model for how DNA might wrap completely around the *Pf*-SSB tetramer is shown in [Figure 5C](#). This proposed path of the ssDNA follows a topology similar to the seams on a baseball as previously found for the *Ec*-SSB-(dC)₃₅ structure¹¹ ([Figure 5D](#)), although the backbone polarity is opposite to that observed in the *Ec*-SSB structure (see below for discussion of polarity).

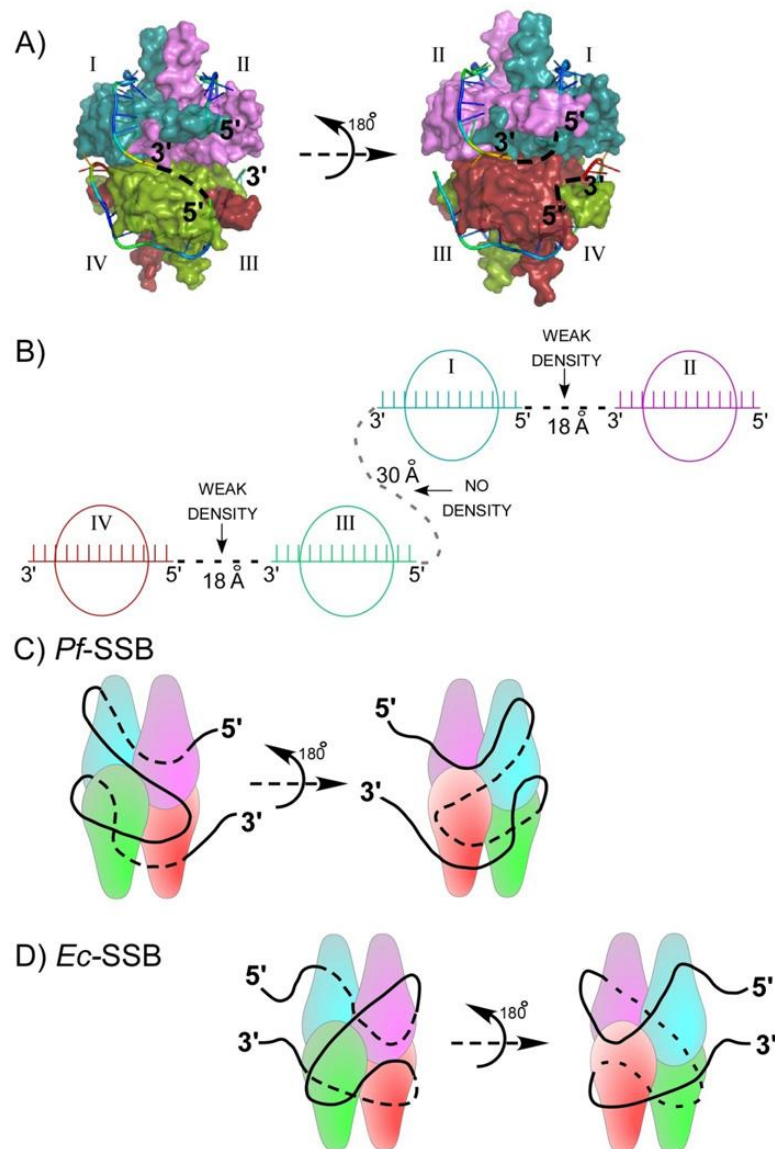


Figure 5
Models for DNA wrapping around *Pf*-SSB

(A) Shows a spaced filled version of the *Pf*-SSB structure with the bound DNA colored according to its B-factor. The predicted path of a (dT)₇₀ DNA molecule is shown by dotted lines traversing across the tetramer and the path of the missing DNA residues in each (dT)₃₅ molecule is also denoted by dotted lines. (B) Is a schematic depicting the polarity of each (dT)₃₅ molecule bound to the four subunits in the *Pf*-SSB tetramer. The black dotted lines represents regions of the DNA for which we observe weak density and the grey dotted lines, connecting the two (dT)₃₅ molecules, is a predicted path for wrapping of a (dT)₇₀ molecule. (C) Is a cartoon representation showing the front and back views of DNA wrapping around the *Pf*-SSB tetramer. (D) Depicts the path of DNA wrapping around the *Ec*-SSB tetramer¹¹.

Based on this crystal structure, we cannot completely exclude the alternate pathway for DNA wrapping around the tetramer, where

the 5' end of the DNA bound to subunit II connects with the 3' end of the DNA bound to subunit III ([Figures 5A and 5B](#)). If this were to be the case, then a 'baseball seam' like topology for wrapping would not hold true. However, to accommodate this alternate path, the 5' end of the DNA bound to subunit II, which is buried within the protein due to the closure of the L₂₋₃ and L₁₋₂ loops must become available, and would require significant movement of both these loops away from each other to facilitate this alternate pathway for wrapping.

We observe ~26 nucleotides bound to each half of the tetramer and the ~ 30 Å gap between the 5' and 3' ends of the DNA can be filled with ~ 5 nucleotides ([Figure 5B](#)). The shorter ~ 18 Å gap would accommodate ~ 3 nucleotides ([Figure 5B](#)), hence ~61– 64 nts of ssDNA would be required to completely wrap around the entire tetramer. Indeed this estimate is consistent with the occluded site size of 62 ± 2 nt for the *Pf*-SSB tetramer on poly (dT) DNA measured under high salt conditions (buffer H^{0.2M}) (Antony *et. al.*, accompanying paper).

We observe excellent density for the DNA in our structure and the 2.1 Å resolution is sufficient to determine the backbone polarity of the DNA bound to *Pf*-SSB. Interestingly, the backbone polarity of the (dT)₃₅ molecules within the *Pf*-SSB complex ([Figure 6A](#)) is opposite to that observed in the *Ec*-SSB-(dC)₃₅ structure ([Figure 6B](#)). In the *Pf*-SSB structure, the 5' end of the DNA binds to the L₁₋₂ loop and is extended through contacts with the L₄₋₅ loop towards loop L₂₋₃ ([Figure 6A](#)). In the DNA bound structures of *Mycobacterium smegmatis* SSB (*Ms*-SSB) (PDB code: 3A5U) and *Helicobacter pylori* SSB (*Hp*-SSB)³⁹, the polarity of the bound DNA is the same as observed in the *Pf*-SSB structure.

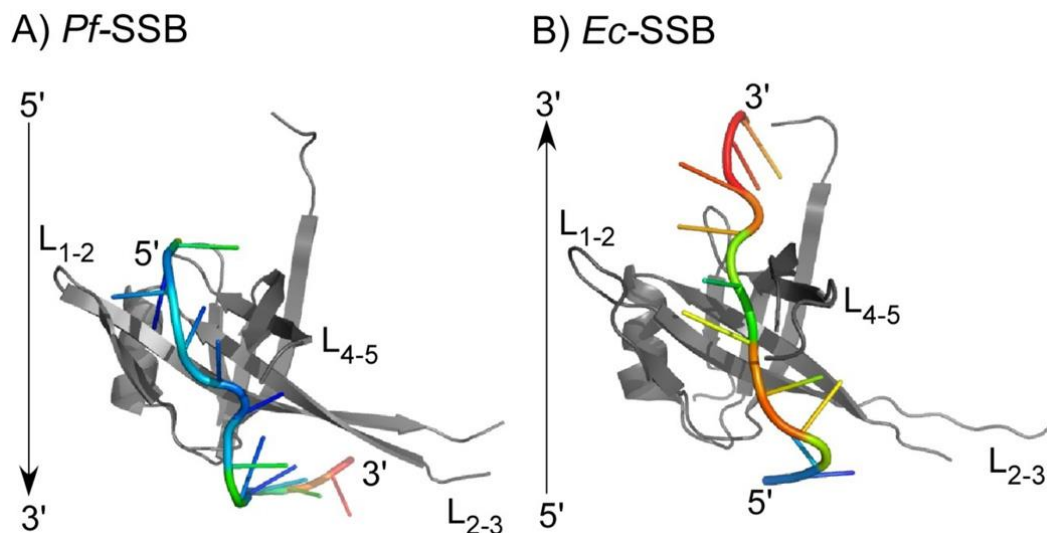


Figure 6: ssDNA wraps around *Pf*-SSB with polarity opposite to *Ec*-SSB
Polarity of the ssDNA bound across a monomer in (A) *Pf*-SSB and (B) *Ec*-SSB. The DNA is bound with a 5'-3' polarity from top to bottom in the *Pf*-SSB structure and with opposite polarity in the *Ec*-SSB structure.

Discussion

We describe a crystal structure of the *Plasmodium falciparum* SSB tetramer bound to ssDNA at 2.1 Å resolution. All four subunits interact with the ssDNA and the topology of the DNA path resembles the “seams of a baseball” as observed for *E. coli* SSB in its fully wrapped (SSB)₆₅ DNA binding mode (Figure S5)¹¹. Although crystal structures of SSB proteins from multiple organisms have been reported in their apo-form, only three SSB-DNA complex structure have been reported. Of these, only the crystal structure of the *Ec*-SSB DNA complex was crystallized with the entire tetramer in the asymmetric unit and density for 26–28 of the 35 nucleotides in each of the two bound (dC)₃₅ DNA molecules was observed thereby providing sufficient information to determine the topology of the wrapped ssDNA¹¹. In the *Pf*-SSB-(dT)₃₅ structure reported here, we also observe electron density for the entire tetramer and for 25–26 nts of each of the two molecules of (dT)₃₅ bound to the protein (Figure S4). We find that ssDNA wraps around the *Pf*-SSB tetramer with a topology similar to *Ec*-SSB, but with opposite polarity. There are three notable differences between the *Pf*-SSB and *Ec*-SSB structures: a) protein-DNA contacts, b) the symmetry of the DNA contacts in the four subunits, and c) the protein-protein contacts between adjacent tetramers. If and

how these factors contribute to the observed difference in polarity of DNA wrapping, DNA binding activity or DNA binding modes remains to be determined (see Antony *et. al.*, accompanying paper).

In the *Pf*-SSB structure, an extensive network of interactions between the amino acid side chains and the bases of the DNA is apparent (Figure 4). These interactions can be divided into stacking interactions between the aromatic protein side chains and the nucleotides, ionic and polar contacts, and contacts between the protein and the phosphate backbone of the DNA. In both the *Ec*-SSB and *Pf*-SSB structures, significant interactions occur through stacking interactions between the bases in the DNA and three tryptophan residues per subunit (W117, W131 and W166 in *Pf*-SSB). The aromatic side chains of these tryptophans stack against the pyrimidine bases T1, T8 and T5, respectively (Figure 4). These residues are also conserved in *Ec*-SSB (W40, W54 and W88) but only two of the three Trp residues (W54 and W88) base stack with similar orientations in all four subunits. W40 is located on the 2–3 loop and adopts multiple conformations in the four subunits of *Ec*-SSB due to the flexible nature of the loop. The homologous W117 residue in *Pf*-SSB is not positioned on the 2–3 loop, but is located on the structured β -sheet 2 and adopts the same conformation in all four subunits. In *Pf*-SSB we observe 98% quenching of the Trp fluorescence upon saturation with two molecules of (dT)₃₅ or one molecule of (dT)₇₀. This is consistent with the observation that all three of the Trp residues in *Pf*-SSB form stacking interactions with the DNA bases and thus the fluorescence of each is essentially fully quenched. *Pf*-SSB also uses a unique set of charged residues to mediate electrostatic interactions with the DNA phosphates. R90, K128, R153 and R154 form electrostatic interactions with the DNA, but these residues are not conserved in *Ec*-SSB (Figure 3). In *Ec*-SSB, Histidine 55 contributes to the stability of the tetramer in that a H55Y mutation (*ssb-1*) destabilizes the tetramer in favor of monomers. This *ssb-1* mutation results in a temperature sensitive phenotype *in vivo*. The homologous residue, H132 in *Pf*-SSB, is also located at the same position and makes *inter*-subunit contacts with N83 and L160 (N6 and L83 are the homologous residues in *Ec*-SSB).

Another difference between the *Ec*-SSB and *Pf*-SSB structures is that the protein-DNA contacts are more symmetric within the *Pf*-SSB complex. In the *Pf*-SSB-(dT)₃₅ structure, the DNA contacts are the

same within each subunit (Figures 3 and 4), whereas in the *Ec*-SSB-(dC)₃₅ structure, a subset of the contacts differ among the subunits¹¹. A part from the conformational differences observed for W40 in the *Ec*-SSB structure, it has been hypothesized that the (SSB)₃₅ binding mode is mediated by the asymmetry in the stacking interaction between the DNA and W54 situated on β 3 extension which is observed in only three of the four subunits¹¹. In *Pf*-SSB, the homologous W166 residue shows stacking interactions within all four subunits of the tetramer. An *E. coli* mutant with either a W54S or W88T mutation shows increased sensitivity to UV, however this is not the case for a W40T substitution⁵¹. However, biochemical studies suggest interactions between W40 and the ssDNA⁵². A W54S mutation also results in a relative stabilization of the (SSB)₃₅ DNA binding mode in *Ec*-SSB³⁶ and in both the *Ec*-SSB and *Pf*-SSB structures this residue forms a stacking interaction with the nucleotide. This suggests that W54 is important for promoting the fully wrapped (SSB)₆₅ DNA binding mode. The *E. coli* *ssb*-3 mutation (G15 to D) shows extreme sensitivity to UV⁵³ and is positioned close to the ssDNA in the crystal structure¹¹. This residue is also conserved in *Pf*-SSB (G92) and is also positioned close to the DNA suggesting a conservation of key amino acid residues between the two proteins.

The third major difference between the two structures lies in the tetramer-tetramer interface between symmetry related molecules (Figure 7). In all *Ec*-SSB structures solved to date, the L₄₋₅ loops from neighboring tetramers pack against each other (Figure 7B). This led to the hypothesis that this tetramer-tetramer interface might be involved in the cooperative (SSB)₃₅ DNA binding mode in *Ec*-SSB¹¹. We do not observe such an interface in the *Pf*-SSB crystals (Figure 7A). As shown in the accompanying paper (Antony *et. al.*), *Pf*-SSB also does not appear able to form a stable (SSB)₃₅ DNA binding mode. The structure and the length of the L₄₋₅ loops in the various apo- or DNA bound crystal structures of homologous bacterial SSB proteins also appears to be similar. In the *Ec*-SSB structures, only the basal half of this loop contacts the DNA. Moreover, the top parts of the L₄₋₅ loops are disordered in all structures except *Ec*-SSB, where they form *inter*-tetrameric contacts that may be important for cooperative binding in the (SSB)₃₅ mode. The conserved size of the L₄₋₅ loop suggests that it may be important for tetramer-tetramer interactions in other SSB homologs as well.

A) *Pf*-SSB

B) *Ec*-SSB

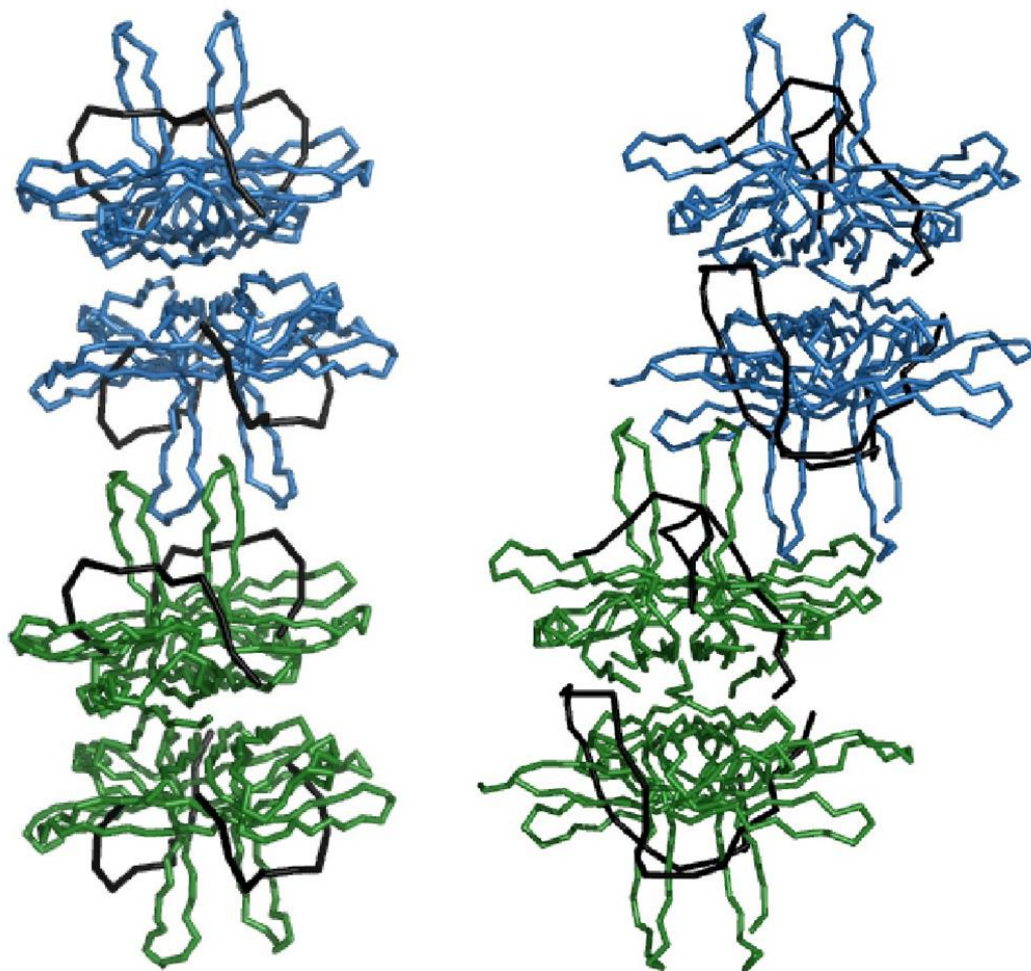


Figure 7: Protein-protein contacts between SSB tetramers

Contacts between tetramers in neighboring unit cells in *Pf*-SSB (A) and *Ec*-SSB (B) are shown. The bound DNA in each structure is represented by the black ribbons.

It is possible that some of these differences may result from the different solution conditions under which the two structures were crystallized. The *Pf*-SSB-(dT)₃₅ crystals only grew in either 0.2 M Na [Br, Cl or SO₄] whereas the *Ec*-SSB-(dC)₃₅ crystals were obtained in the absence of any added salt¹¹. Multiple DNA binding modes have been observed with *Ec*-SSB that are dependent upon the salt concentration. The (SSB)₃₅ DNA binding mode is observed at low NaCl concentrations (< 10 mM), whereas the fully wrapped (SSB)₆₅ binding mode is observed at higher NaCl concentrations (> 200 mM)¹³. Our attempts to obtain crystals of *Pf*-SSB-(dT)₃₅ complexes under the low

salt conditions used to obtain the *Ec*-SSB-dC₃₅ crystals were not successful.

A final striking difference between the *Pf*- and *Ec*-SSB proteins is the sequence divergence of the unstructured C-terminus and the composition of the C-terminal amino acid end (*Pf*: MNVQEFEE versus *Ec*: DFDDDIPF). However, it is not likely that this region plays a role in determining the polarity of the bound ssDNA. In *Plasmodium*, compounds inhibiting the activity of apicoplast proteins have been used as successful anti-malarial drugs⁵⁴. Mutations in the *Ec*-SSB C-terminus render *E. coli* severely impaired for DNA repair and replication or result in lethality⁸. Small molecule inhibitors that inhibit the interaction of the *E. coli* SSB C-terminal tails with an array of other proteins have emerged as a new class of potential antibiotics⁵⁵. It remains to be determined whether the sequence of the *Pf*-SSB C-terminus is important for any *Pf*-SSB interactions with any proteins important for its function in the apicoplast, although this possibility seems likely.

Materials and Methods

Buffers

Buffer H^{0.08} is 10 mM Hepes, pH 8.1, 1 mM EDTA, 0.08 M NaCl and 1 mM tris(2-carboxyethyl)phosphine (TCEP). Buffer H^{0.2} is 10 mM Hepes, pH 8.1, 0.1 mM Na₃EDTA, 200 mM NaCl and 5 mM 2-ME. Lysis buffer is 50 mM Tris-Cl, pH 8.3, 1 mM EDTA, 200 mM NaCl, 10% sucrose, and 15 mM spermidine. Buffer T^x is 50 mM Tris-Cl, pH 8.3, 1 mM EDTA, 5 % (v/v) glycerol, where "x" denotes the molar concentration of NaCl. Storage buffer is 20 mM Tris-Cl, pH 8.3, 1 mM Na₃EDTA, 500 mM NaCl, 5 mM 2-mercaptoethanol, 50% (v/v) glycerol.

Expression and Purification of Pf-SSB

The *Pf*-SSB gene was amplified from genomic DNA (3D7 isolate, a kind gift from Dr. Daniel Goldberg, Washington University) using the following primers: Forward: 5'-AATTCATATGAATGAGAAATCATTAAT-3' and Reverse: 5'-AATTGGATCCTCATTCTTCAAATTCTTGG -3', and cloned into the pET21a vector (Novagen Inc.) using *NdeI* and *BamHI*

restriction sites. The DNA encoding for the N-terminal amino acids 1–76 was omitted since it encodes the apicoplast localization signal (ALS)⁴. Furthermore, constructs containing the ALS signal sequence did not overexpress in *E. coli*. We refer to this version of *Pf*-SSB (residues 77–284) that lacks the ALS signal sequence as the wild type protein.

Pf-SSB was overexpressed in BL21(DE3) cells and purified using a procedure similar to that described for *E. coli* SSB. All steps were carried out at 4°C. 30 g of cell paste was resuspended in lysis buffer (150 mL) and lysed using an Avestin cell disrupter (Avestin Inc., Canada) and *Pf*-SSB and DNA in the clarified lysate were precipitated by adding polyethyleneimine (PEI) to 0.2% (final). The protein was resuspended from the PEI pellet using 200 ml of buffer T^{0.4}. *Pf*-SSB from the PEI-resuspension was precipitated by adding solid ammonium sulfate (144 g/L) (25% saturation) and the pellet containing >90 % pure *Pf*-SSB was resuspended in buffer T^{0.3} (200 mL). The resuspended protein was loaded onto a ssDNA cellulose column (50 mL resin with ~3 mg/mL binding capacity) and eluted using a linear NaCl gradient (0.3 – 2 M) in buffer T. Fractions containing *Pf*-SSB were pooled and precipitated with 30.8% ammonium sulfate (170 g/L). The resulting precipitate was resuspended in 10 mL of storage buffer, dialyzed and stored as 0.5 mL aliquots at –20°C. The concentration of *Pf*-SSB was determined spectrophotometrically using an extinction coefficient of $\epsilon_{280} = 9.58 \times 10^4 \text{ M}^{-1} \text{ (tetramer) cm}^{-1}$. Using this procedure the typical yield of *Pf*-SSB is around 15 mg per gram of cell paste. The extinction coefficient in buffer H^{0.2} and T^{0.2} was determined by comparing the absorbance of *Pf*-SSB in buffer H^{0.2} and T^{0.2} with its absorbance in 6 M Guanidium-HCl, 10 mM Tris-Cl, pH 8.1, 0.25 mM Na₃EDTA, and 1 mM 2-mercaptoethanol at 25°C. The extinction coefficient of the denatured *Pf*-SSB in 6 M Guanidinium HCl was calculated as the sum of the extinction coefficients of the 3 Trp, 4 Tyr and 3 Phe in 6 M Guanidinium HCl⁵². *Pf*-SSB was dialyzed extensively at 4°C versus the buffers used in each experiment using a 10,000 Da molecular weight cut-off dialysis membrane (Spectrum Inc., Houston, TX). *Pf*-SSB has a single exposed cysteine and in the absence of reducing agent (5 mM 2-mercaptoethanol or 1 mM TCEP (tris(2-carboxyethyl)phosphine)) it forms higher order oligomers in solution (Figure S1). For this reason, all experiments were performed in the presence of 1 mM TCEP.

DNA

The oligodeoxynucleotides, (dT)₃₅ and (dT)₇₀, were synthesized and purified as described⁵⁸. All ssDNA concentrations were determined spectrophotometrically using the extinction coefficient $\epsilon_{260} = 8.1 \times 10^3 \text{ M}^{-1} (\text{nucleotide}) \text{ cm}^{-1}$ for oligo (dT) in buffer H^{0.08}.

Analytical Ultracentrifugation

Sedimentation experiments were performed using an Optima XL-A analytical ultracentrifuge equipped with an An50Ti rotor (Beckman Coulter, Fullerton, CA) at 25°C. For sedimentation equilibrium experiments, 120 μL of protein solution was loaded into each of the three channels of an Epon charcoal-filled six-channel centerpiece with 130 μL of buffer in each reference channels. Protein concentration was monitored by absorbance at 280 nm at three different protein concentrations (1.04 μM , 3.13 μM and 6 μM Pf-SSB in buffer H^{0.1M}). Data were collected with a spacing of 0.001 cm with an average of ten scans per step at three rotor speeds: 9500, 11500, and 14000 rpm. At each speed sedimentation equilibrium was determined when successive scans measured over a 2 hour time window were super imposable. Data sets were edited and extracted using SEDFIT followed by analysis by nonlinear least squares (NLLS) using the program SEDPHAT⁵⁹. Apparent molecular weights were obtained by fitting the data to eq 1:

$$A_T = \sum_{i=1}^n \exp(\ln A_{0,i} + \sigma_i)(r^2 - r_{ref}^2)/2 + b \quad (1)$$

where A_T is the total absorbance at radial position r , $A_{0,i}$ is the absorbance of component i at the reference radial position (r_{ref}), b is the baseline offset, $\sigma_i = [M_i(1 - \bar{\partial}_i \rho)\omega^2]/RT$, M_i and $\bar{\partial}_i$ are the molecular mass and partial specific volume of component i , respectively (calculated using SEDENTREP⁶⁰). For Pf-SSB the $\bar{\partial}_i$ value (0.7191 mL g⁻¹ at 25°C) was calculated based on its amino acid composition (residues 77–284). The solution density ρ for buffer H^{0.1M} was 1.0026 (calculated using SEDENTREP). ω is the angular velocity, R is the ideal gas constant and T is the absolute temperature. A global NLLS fit to eq

1 of the nine absorbance files was used to calculate the molecular weight.

Sedimentation velocity experiments ([Figure 3B](#)), were performed using 3 μM *Pf*-SSB alone or in complex with 3 μM (dT)₇₀ (1:1 molar ratio) or 6 μM (dT)₃₅ (1:2 molar ratio). Experiments were also performed on both (dT)₇₀ and (dT)₃₅ DNA molecules alone. 380 μL of sample and 392 μL of buffer were loaded into the appropriate sectors of an Epon charcoal-filled two-sector centerpiece and centrifuged at 42000 rpm (25°C) and the absorbance was monitored at 280 nm. The continuous sedimentation coefficient distribution, $c(s)$, was calculated using the program SEDFIT.

DNA Binding

Pf-SSB binding to the oligodeoxynucleotides, (dT)₇₀ or (dT)₃₅, was monitored by the quenching of the intrinsic Trp fluorescence of *Pf*-SSB using a PTI QM-2000 fluorometer (Photon Technologies, Inc., Lawrenceville, NJ) [λ_{ex} = 296 nm, 2 nm excitation band-pass, and λ_{em} = 345 nm, 2–5 nm emission band-pass] with corrections applied as described previously⁵⁷. The experiments were performed in Buffer H^{0.2} at 25°C using either 0.1 or 0.3 μM *Pf*-SSB tetramer. Under these conditions, the binding affinities of *Pf*-SSB for (dT)₇₀ and (dT)₃₅ are too large to measure (i.e., the titrations were stoichiometric) and the intersection of the linear parts of the titration curves was used to determine the stoichiometry of DNA binding per *Pf*-SSB tetramer.

Crystallization and Structure Determination

Pf-SSB (6 mg/ml: 61 μM tetramer) was mixed with 122 μM (dT)₃₅ (1:2 ratio) in buffer H^{0.2} (10 mM Hepes, pH 8.1, 0.1 mM Na₃EDTA, 200 mM NaCl and 5 mM 2-mercaptoethanol) and dialyzed extensively vs. buffer H^{0.2} at 4°C. The concentration of protein after dialysis was \sim 3 mg/mL. Crystals were grown by vapor diffusion using the sitting drop method in 96-well plates using a crystallization robot (Phoenix – Art Robbins Instruments, Sunnyvale, CA). The first *Pf*-SSB-(dT)₃₅ crystal form (bi-pyramidal) was observed in several commercial PEG based screens (PEG/Ion HT - Hampton Research, Aliso Viejo, CA, PEGs Suite – Qiagen, Valencia, CA, and PACT premier - Molecular

Dimensions, Apopka, FL) at 20°C after 3–4 days. The second *Pf*-SSB-(dT)₃₅ crystal form (long rods) was observed at 4°C after 4–5 weeks in 0.1 M Bis-Tris Propane, pH 8.5, 20 % PEG 3350 and either 0.2 M sodium bromide or 0.2 M sodium sulfate. Crystals of a *Pf*-SSB-(dT)₃₅ complex, grown in 0.1 M Bis-Tris Propane, pH 8.5, 0.15 M sodium sulfate and 24 % PEG 3350 at 15°C, were harvested into cryo-protectant solution (20 % ethylene glycol, 5 % PEG 3350 and 60 % mother liquor) and flash frozen in liquid nitrogen. Diffraction data were collected using a 1.2 kW MM007 Rigaku generator with VHF optics and Raxis-IV++ image detector under cryo-stream with the X-stream cryo-cooling system. Data were processed with the HKL2000 program⁶¹. Initial phases were obtained by the molecular replacement method using Phaser within the CCP4i program suit using the structure of the *E. coli* SSB/DNA complex¹¹ (PDB code 1EYG).

Initial bi-pyramidal crystals belonging to the tetragonal space group I422 with unit cell parameters $a = b = 83.1$, and $c = 136.7$ Å contained one *Pf*-SSB monomer per asymmetric unit. A second crystal form was also obtained belonging to a monoclinic space group (Table 1) with one tetramer per asymmetric unit. Since the structure of the monomer in the tetragonal group was close to that of the monoclinic form, we describe the structure of the tetramer. The model building and refinement were completed using Arp/Warp⁶⁶, Coot⁶⁷ and Refmac⁶⁸. Non-crystallographic averaging was not utilized during the initial model building and refinement steps. The following residues were disordered and not modeled due to poor electron density: chain A 169–172, chain B 121 and 171–173, chain C 170–171 and chain D 121–122 and 169–171. The model was refined to a resolution of 2.1 Å with $R = 22.8$ and Free $R = 27.5$ with excellent geometry (Table 1).

Table 1: Data collection and refinement statistics.

Space group	C2
Unit cell (Å)	$a = 118.0$; $b = 82.8$; $c = 87.6$; $d = 99.57$
Data collection resolution	50–2.1
R-merge (%) [*]	6.8 (52.9)
Completeness [*]	99.4 (97.3)
I/σ high resolution shell	3
Refinement resolution (Å)	30–2.1
# protein non-H atoms	3638
# DNA atoms	1022
# water molecules	232

Space group	C2
# reflections	45791
# reflection test set (5%)	2438
R (%) [*]	21.8 (28.3)
Free R (%) [*]	27.6 (35.4)
Rmsd bonds (Å)	0.01
Angles	1.5
Overall B factor, protein (Å ²)	35
Overall B factor, DNA (Å ²)	57
Overall B factor, solvent (Å ²)	43
Ramachandran plot ^{**}	
Most favored regions (%)	90.0
Allowed regions (%)	9.0
Generously allowed (%) ^{***}	1.0
Disallowed (%)	0.0

*Values for highest resolution for data collection 2.10–2.14, and for refinement 2.10–2.15 Å are shown in parentheses.

**Ramachandran plot parameters were calculated by program PROCHECK⁶⁹

***Residues in generously allowed conformation are in poorly structured loops.

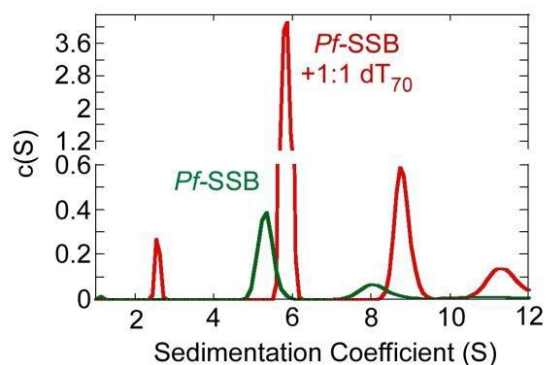
Highlights

- DNA binding properties of *Plasmodium falciparum* SSB are different from *E. coli* SSB.
- Unlike *Ec*-SSB, the *Pf*-SSB does not possess the (SSB)₃₅ DNA binding mode.
- *Pf*-SSB has unique DNA binding properties.
- *Pf*-SSB DNA binding activity might be specific for biological function in *Plasmodium*.

Supplemental Information

Figure S1

A) Buffer H + 200 mM NaCl (No reducing agent)



B) Buffer H + 200 mM NaCl + 1mM TCEP

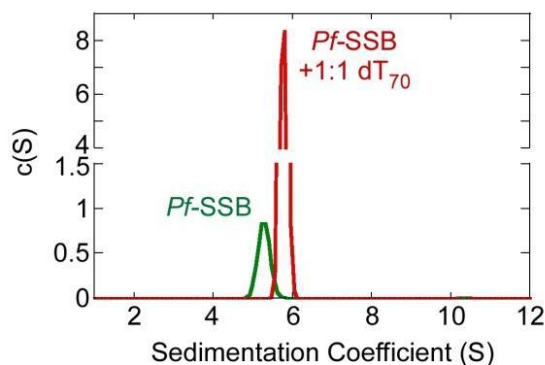


Figure S1. *Pf*-SSB forms higher order complexes in the absence of reducing agents. A) Analytical sedimentation velocity centrifugation analysis of *Pf*-SSB (3 μ M) in the absence (green) or presence (red) of (dT)₇₀ DNA (3 μ M). $c(s)$ profiles measured in buffer H with 200 mM NaCl in the absence of reducing agents reveal presence of multiple peaks which correspond to formation of homotetramers, octamers and higher order species. (B) Addition of 1 mM TCEP to the reaction results in the formation of a discrete single peak corresponding to a homotetramer.

Figure S2

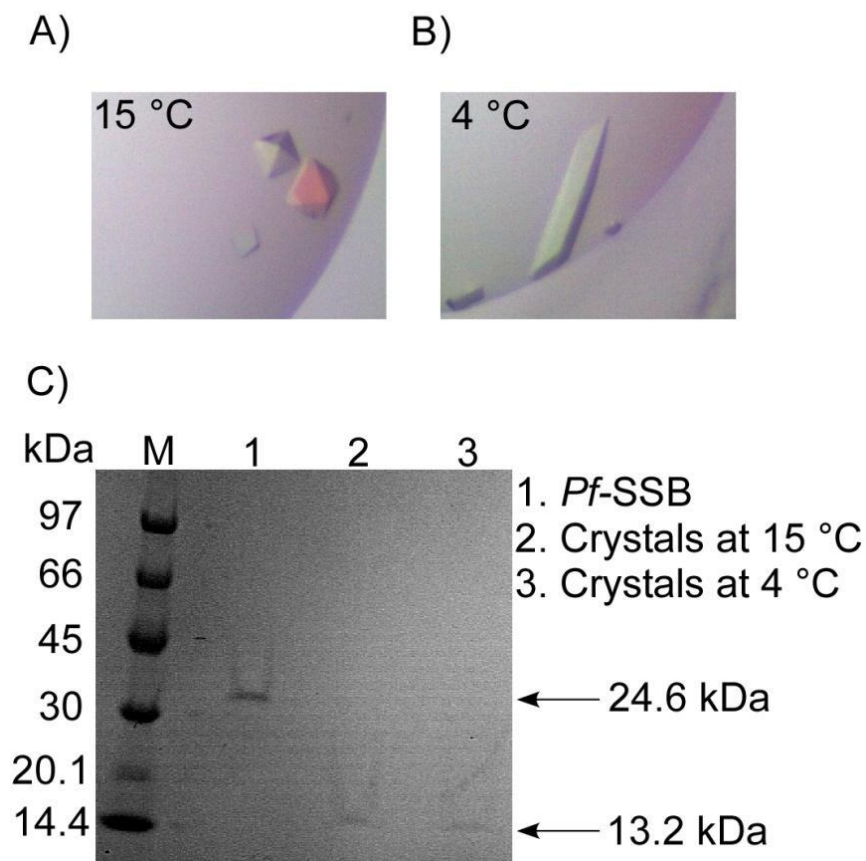


Figure S2. Crystals of the *Pf*-SSB-(dT)35 complex that was grown at either 15°C (A) or 4°C (B). (C) Crystals were collected into loading buffer and analyzed on a SDS PAGE gel. The faster migrating bands in the samples from the crystals compared to the control sample suggest proteolytic cleavage during crystallization. Note that full length *Pf*-SSB sample (lane 1) migrates slower than expected, possibly due to poor interaction of its asparagine rich Cterminus with SDS in the buffer.

Figure S3

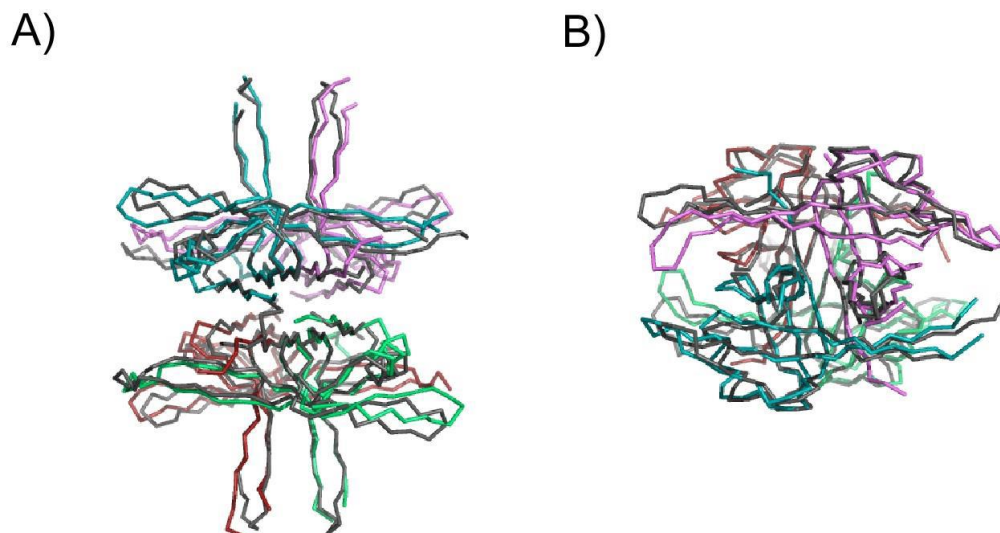


Figure S3. (A) Front and (B) top view of the superimposition of the *Pf*-SSB and *Ec*-SSB homotetramer structures show the high degree of structural similarity between the two proteins.

Figure S4

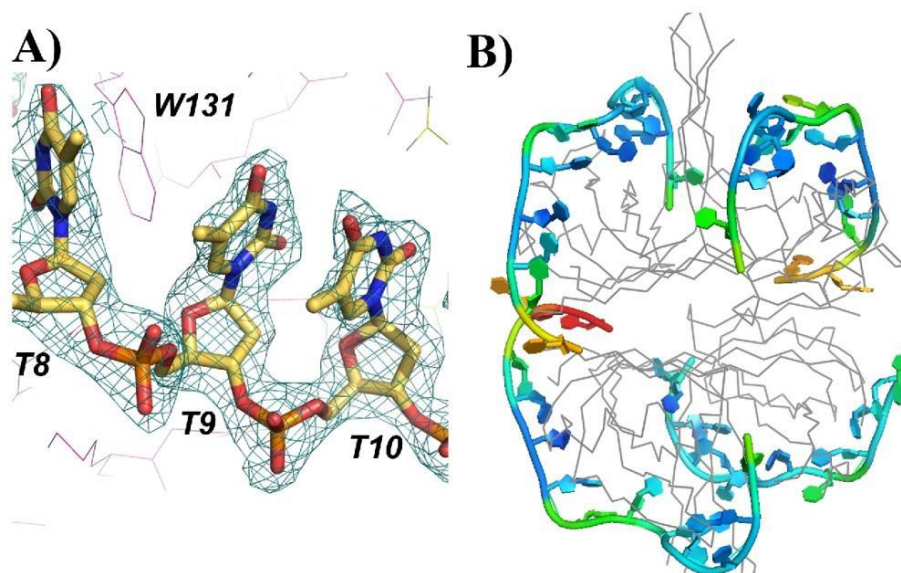


Figure S4. A) A representative region of 2Fobs-Fcalc composite omit electron-density map contoured around ssDNA at 1 σ level and calculated using CNS simulated annealing omit map protocol. B) Ribbon diagram of ssDNA color-coded according to B-factor in spectrum from blue for lowest B-factor atoms to red with the highest B-factor.

Figure S5

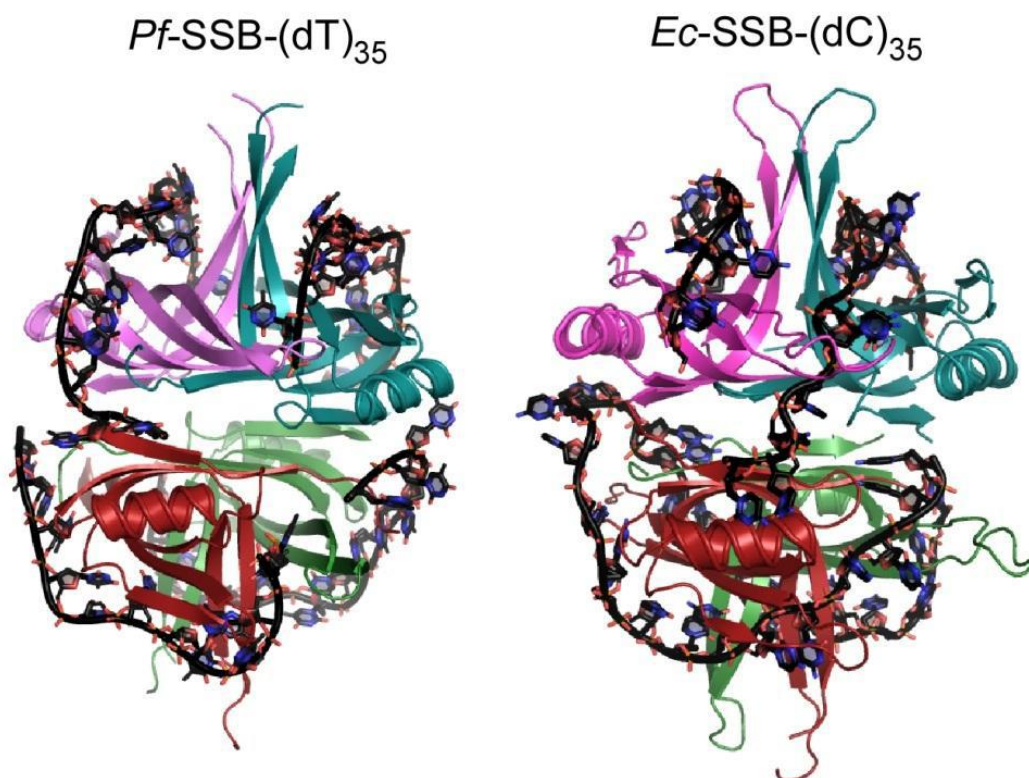


Figure S5. Comparison of ssDNA wrapping around the *Pf*-SSB and *Ec*-SSB proteins. The individual subunits are shown as ribbons and the DNA is shown as sticks.

Acknowledgements

The *Plasmodium falciparum* genomic DNA was a kind gift from Dr. Daniel Goldberg (Washington University School of Medicine). We thank Drs. Alex Kozlov and Binh Nguyen for significant technical advice. Thang Ho for synthesis and purification of the oligodeoxynucleotides. This work was supported in part by grants from the NIH to T.M.L. (GM30498, GM45948) and S.K. (GM073837).

Abbreviations

SSB	Single strand DNA binding protein
ssDNA	single stranded DNA
dsDNA	double stranded DNA

<i>Pf</i> -SSB	<i>Plasmodium falciparum</i> SSB
<i>Ec</i> -SSB	<i>Escherichia coli</i> SSB
SIPs	SSB interacting proteins

Footnotes

Publisher's Disclaimer: This is a PDF file of an unedited manuscript that has been accepted for publication. As a service to our customers we are providing this early version of the manuscript. The manuscript will undergo copyediting, typesetting, and review of the resulting proof before it is published in its final citable form. Please note that during the production process errors may be discovered which could affect the content, and all legal disclaimers that apply to the journal pertain.

Accession Numbers: The coordinates of the *Pf*-SSB-(dT)₃₅ complex have been deposited in the Protein Data Bank with PDB ID: **3ULP**.

References

1. Snow RW, Guerra CA, Noor AM, Myint HY, Hay SI. The global distribution of clinical episodes of *Plasmodium falciparum* malaria. *Nature*. 2005;434:214–217.
2. Wilson RJ, Denny PW, Preiser PR, Rangachari K, Roberts K, Roy A, Whyte A, Strath M, Moore DJ, Moore PW, Williamson DH. Complete gene map of the plastid-like DNA of the malaria parasite *Plasmodium falciparum*. *J Mol Biol*. 1996;261:155–172.
3. Dahl EL, Rosenthal PJ. Apicoplast translation, transcription and genome replication: targets for antimalarial antibiotics. *Trends Parasitol*. 2008;24:279–284.
4. Prusty D, Dar A, Priya R, Sharma A, Dana S, Choudhury NR, Rao NS, Dhar SK. Single-stranded DNA binding protein from human malarial parasite *Plasmodium falciparum* is encoded in the nucleus and targeted to the apicoplast. *Nucleic Acids Res*. 2010;38:7037–7053.
5. Lohman TM, Ferrari ME. *Escherichia coli* single-stranded DNA-binding protein: multiple DNA-binding modes and cooperativities. *Annu Rev Biochem*. 1994;63:527–570.
6. Lohman TM, Bujalowski W, Overman LB. *E. coli* single strand binding protein: a new look at helix-destabilizing proteins. *Trends Biochem Sci*. 1988;13:250–255.
7. Sancar A, Williams KR, Chase JW, Rupp WD. Sequences of the *ssb* gene and protein. *Proc Natl Acad Sci U S A*. 1981;78:4274–4278.

8. Shereda RD, Kozlov AG, Lohman TM, Cox MM, Keck JL. SSB as an organizer/mobilizer of genome maintenance complexes. *Crit Rev Biochem Mol Biol.* 2008;43:289–318.
9. Chrysogelos S, Griffith J. Escherichia coli single-strand binding protein organizes single-stranded DNA in nucleosome-like units. *Proc Natl Acad Sci U S A.* 1982;79:5803–5807.
10. Lohman TM, Overman LB. Two binding modes in Escherichia coli single strand binding protein-single stranded DNA complexes. Modulation by NaCl concentration. *J Biol Chem.* 1985;260:3594–3603.
11. Raghunathan S, Kozlov AG, Lohman TM, Waksman G. Structure of the DNA binding domain of E. coli SSB bound to ssDNA. *Nat Struct Biol.* 2000;7:648–652.
12. Bujalowski W, Lohman TM. Escherichia coli single-strand binding protein forms multiple, distinct complexes with single-stranded DNA. *Biochemistry.* 1986;25:7799–7802.
13. Bujalowski W, Overman LB, Lohman TM. Binding mode transitions of Escherichia coli single strand binding protein-single-stranded DNA complexes. Cation, anion, pH, binding density effects. *J Biol Chem.* 1988;263:4629–4640.
14. Lohman TM, Overman LB, Datta S. Salt-dependent changes in the DNA binding co-operativity of Escherichia coli single strand binding protein. *J Mol Biol.* 1986;187:603–615.
15. Bujalowski W, Lohman TM. Limited co-operativity in protein-nucleic acid interactions. A thermodynamic model for the interactions of Escherichia coli single strand binding protein with single-stranded nucleic acids in the "beaded", (SSB)₆₅ mode. *J Mol Biol.* 1987;195:897–907.
16. Griffith JD, Harris LD, Register J., 3rd Visualization of SSB-ssDNA complexes active in the assembly of stable RecA-DNA filaments. *Cold Spring Harb Symp Quant Biol.* 1984;49:553–559.
17. Roy R, Kozlov AG, Lohman TM, Ha T. Dynamic structural rearrangements between DNA binding modes of E. coli SSB protein. *J Mol Biol.* 2007;369:1244–1257.
18. Roy R, Kozlov AG, Lohman TM, Ha T. SSB protein diffusion on single-stranded DNA stimulates RecA filament formation. *Nature.* 2009;461:1092–1097.
19. Shamoo Y, Friedman AM, Parsons MR, Konigsberg WH, Steitz TA. Crystal structure of a replication fork single-stranded DNA binding protein (T4 gp32) complexed to DNA. *Nature.* 1995;376:362–366.
20. Bernstein DA, Eggington JM, Killoran MP, Misic AM, Cox MM, Keck JL. Crystal structure of the Deinococcus radiodurans single-stranded DNA-binding protein suggests a mechanism for coping with DNA damage. *Proc Natl Acad Sci U S A.* 2004;101:8575–8580.

21. Wold MS. Replication protein A: a heterotrimeric, single-stranded DNA-binding protein required for eukaryotic DNA metabolism. *Annu Rev Biochem.* 1997;66:61–92.
22. Norais CA, Chitteni-Pattu S, Wood EA, Inman RB, Cox MM. DdrB protein, an alternative *Deinococcus radiodurans* SSB induced by ionizing radiation. *J Biol Chem.* 2009;284:21402–21411.
23. Dam J, Schuck P. Calculating sedimentation coefficient distributions by direct modeling of sedimentation velocity concentration profiles. *Methods Enzymol.* 2004;384:185–212.
24. Schuck P. Sedimentation analysis of noninteracting and self-associating solutes using numerical solutions to the Lamm equation. *Biophys J.* 1998;75:1503–1512.
25. Krauss G, Sindermann H, Schomburg U, Maass G. *Escherichia coli* single-strand deoxyribonucleic acid binding protein: stability, specificity, and kinetics of complexes with oligonucleotides and deoxyribonucleic acid. *Biochemistry.* 1981;20:5346–5352.
26. Bujalowski W, Lohman TM. Negative co-operativity in *Escherichia coli* single strand binding protein-oligonucleotide interactions. II. Salt, temperature and oligonucleotide length effects. *J Mol Biol.* 1989;207:269–288.
27. Lohman TM, Bujalowski W. Negative cooperativity within individual tetramers of *Escherichia coli* single strand binding protein is responsible for the transition between the (SSB)₃₅ and (SSB)₅₆ DNA binding modes. *Biochemistry.* 1988;27:2260–2265.
28. Bujalowski W, Lohman TM. Negative co-operativity in *Escherichia coli* single strand binding protein-oligonucleotide interactions. I. Evidence and a quantitative model. *J Mol Biol.* 1989;207:249–268.
29. Gallagher JR, Matthews KA, Prigge ST. *Plasmodium falciparum* apicoplast transit peptides are unstructured in vitro and during apicoplast import. *Traffic.* 2011;12:1124–1138.
30. McFadden GI. Plastids and protein targeting. *J Eukaryot Microbiol.* 1999;46:339–346.
31. Ng JD, McPherson A. Preliminary crystallographic analysis of a proteolytically modified form of *E. coli* single stranded DNA binding protein. *J Biomol Struct Dyn.* 1989;6:1071–1076.
32. Thorn JM, Carr PD, Chase JW, Dixon NE, Ollis DL. Crystallization and low temperature diffraction studies of the DNA binding domain of the single-stranded DNA binding protein from *Escherichia coli*. *J Mol Biol.* 1994;240:396–399.
33. Ollis D, Brick P, Abdel-Meguid SS, Murthy K, Chase JW, Steitz TA. Crystals of *Escherichia coli* single-strand DNA-binding protein show that the tetramer has D₂ symmetry. *J Mol Biol.* 1983;170:797–800.

34. Murzin AG. OB (oligonucleotide/oligosaccharide binding)-fold: common structural and functional solution for non-homologous sequences. *EMBO J.* 1993;12:861–867.
35. Curth U, Bayer I, Greipel J, Mayer F, Urbanke C, Maass G. Amino acid 55 plays a central role in tetramerization and function of Escherichia coli single-stranded DNA binding protein. *Eur J Biochem.* 1991;196:87–93.
36. Curth U, Greipel J, Urbanke C, Maass G. Multiple binding modes of the single-stranded DNA binding protein from Escherichia coli as detected by tryptophan fluorescence and site-directed mutagenesis. *Biochemistry.* 1993;32:2585–2591.
37. Ferrari ME, Fang J, Lohman TM. A mutation in E. coli SSB protein (W54S) alters intra-tetramer negative cooperativity and inter-tetramer positive cooperativity for single-stranded DNA binding. *Biophys Chem.* 1997;64:235–251.
38. Carlini LE, Porter RD. Analysis of ssb mutations in vivo implicates SSB protein in two distinct pathways of SOS induction and in recombinational DNA repair. *Mol Microbiol.* 1997;24:129–139.
39. Chan KW, Lee YJ, Wang CH, Huang H, Sun YJ. Single-stranded DNA-binding protein complex from Helicobacter pylori suggests an ssDNA-binding surface. *J Mol Biol.* 2009;388:508–519.
40. Raghunathan S, Ricard CS, Lohman TM, Waksman G. Crystal structure of the homo-tetrameric DNA binding domain of Escherichia coli single-stranded DNA-binding protein determined by multiwavelength x-ray diffraction on the selenomethionyl protein at 2.9-Å resolution. *Proc Natl Acad Sci U S A.* 1997;94:6652–6657.
41. Fedorov R, Witte G, Urbanke C, Manstein DJ, Curth U. 3D structure of Thermus aquaticus single-stranded DNA-binding protein gives insight into the functioning of SSB proteins. *Nucleic Acids Res.* 2006;34:6708–6717.
42. Kaushal PS, Singh P, Sharma A, Muniyappa K, Vijayan M. X-ray and molecular-dynamics studies on Mycobacterium leprae single-stranded DNA-binding protein and comparison with other eubacterial SSB structures. *Acta Crystallogr D Biol Crystallogr.* 2010;66:1048–1058.
43. Saikrishnan K, Jeyakanthan J, Venkatesh J, Acharya N, Sekar K, Varshney U, Vijayan M. Structure of Mycobacterium tuberculosis single-stranded DNA-binding protein. Variability in quaternary structure and its implications. *J Mol Biol.* 2003;331:385–393.
44. Yang C, Curth U, Urbanke C, Kang C. Crystal structure of human mitochondrial single-stranded DNA binding protein at 2.4 Å resolution. *Nat Struct Biol.* 1997;4:153–157.
45. Yadav T, Carrasco B, Myers AR, George NP, Keck JL, Alonso JC. Genetic recombination in Bacillus subtilis: a division of labor between two single-strand DNA-binding proteins. *Nucleic Acids Res.* 2012

46. Bujalowski W, Lohman TM. Monomers of the Escherichia coli SSB-1 mutant protein bind single-stranded DNA. *J Mol Biol.* 1991;217:63–74.
47. Williams KR, Murphy JB, Chase JW. Characterization of the structural and functional defect in the Escherichia coli single-stranded DNA binding protein encoded by the ssb-1 mutant gene. Expression of the ssb-1 gene under lambda pL regulation. *J Biol Chem.* 1984;259:11804–11811.
48. Bujalowski W, Lohman TM. Monomer-tetramer equilibrium of the Escherichia coli ssb-1 mutant single strand binding protein. *J Biol Chem.* 1991;266:1616–1626.
49. Meyer RR, Glassberg J, Scott JV, Kornberg A. A temperature-sensitive single-stranded DNA-binding protein from Escherichia coli. *J Biol Chem.* 1980;255:2897–2901.
50. Meyer RR, Glassberg J, Kornberg A. An Escherichia coli mutant defective in single-strand binding protein is defective in DNA replication. *Proc Natl Acad Sci U S A.* 1979;76:1702–1705.
51. Carlini LE, Porter RD, Curth U, Urbanke C. Viability and preliminary in vivo characterization of site-directed mutants of Escherichia coli single-stranded DNA-binding protein. *Mol Microbiol.* 1993;10:1067–1075.
52. Khamis MI, Casas-Finet JR, Maki AH, Murphy JB, Chase JW. Investigation of the role of individual tryptophan residues in the binding of Escherichia coli single-stranded DNA binding protein to single-stranded polynucleotides. A study by optical detection of magnetic resonance and site-selected mutagenesis. *J Biol Chem.* 1987;262:10938–10945.
53. Meyer RR, Laine PS. The single-stranded DNA-binding protein of Escherichia coli. *Microbiol Rev.* 1990;54:342–380.
54. McFadden GI, Roos DS. Apicomplexan plastids as drug targets. *Trends Microbiol.* 1999;7:328–333.
55. Lu D, Bernstein DA, Satyshur KA, Keck JL. Small-molecule tools for dissecting the roles of SSB/protein interactions in genome maintenance. *Proc Natl Acad Sci U S A.* 2010;107:633–638.
56. Lohman TM, Green JM, Beyer RS. Large-scale overproduction and rapid purification of the Escherichia coli ssb gene product. Expression of the ssb gene under lambda PL control. *Biochemistry.* 1986;25:21–25.
57. Lohman TM, Mascotti DP. Nonspecific ligand-DNA equilibrium binding parameters determined by fluorescence methods. *Methods Enzymol.* 1992;212:424–458.
58. Ferrari ME, Bujalowski W, Lohman TM. Co-operative binding of Escherichia coli SSB tetramers to single-stranded DNA in the (SSB)₃₅ binding mode. *J Mol Biol.* 1994;236:106–123.
59. Vistica J, Dam J, Balbo A, Yikilmaz E, Mariuzza RA, Rouault TA, Schuck P. Sedimentation equilibrium analysis of protein interactions with global

- implicit mass conservation constraints and systematic noise decomposition. *Anal Biochem.* 2004;326:234–256.
60. Laue TM, Shah BD, RIDgeway TM, Pelletier SL. Computer-aided interpretation of analytical sedimentation data for proteins. Royal Society of Cambridge, Cambridge, U.K. 1992;1
61. Otwinowski ZaMW. Processing of X-ray diffraction data collected in oscillation mode. *Macromolecular Crystallography, Pt A.* 1997;276
62. McCoy AJ, Grosse-Kunstleve RW, Adams PD, Winn MD, Storoni LC, Read RJ. Phaser crystallographic software. *J Appl Crystallogr.* 2007;40:658–674.
63. McCoy AJ. Solving structures of protein complexes by molecular replacement with Phaser. *Acta Crystallogr D Biol Crystallogr.* 2007;63:32–41.
64. Potterton E, Briggs P, Turkenburg M, Dodson E. A graphical user interface to the CCP4 program suite. *Acta Crystallogr D Biol Crystallogr.* 2003;59:1131–1137.
65. Winn MD, Ballard CC, Cowtan KD, Dodson EJ, Emsley P, Evans PR, Keegan RM, Krissinel EB, Leslie AG, McCoy A, McNicholas SJ, Murshudov GN, Pannu NS, Potterton EA, Powell HR, Read RJ, Vagin A, Wilson KS. Overview of the CCP4 suite and current developments. *Acta Crystallogr D Biol Crystallogr.* 2011;67:235–242.
66. Langer G, Cohen SX, Lamzin VS, Perrakis A. Automated macromolecular model building for X-ray crystallography using ARP/wARP version 7. *Nat Protoc.* 2008;3:1171–1179.
67. Emsley P, Lohkamp B, Scott WG, Cowtan K. Features and development of Coot. *Acta Crystallogr D Biol Crystallogr.* 2010;66:486–501.
68. Winn MD, Murshudov GN, Papiz MZ. Macromolecular TLS refinement in REFMAC at moderate resolutions. *Methods Enzymol.* 2003;374:300–321.
69. Laskowski RA, Moss DS, Thornton JM. Main-chain bond lengths and bond angles in protein structures. *J Mol Biol.* 1993;231:1049–1067.